J Mater Sci (2008) 43:5350–5357
DOI 10.1007/s10853-008-2783-y

Influence of heat treatment on creep of a Mn–N stabilised austenitic stainless steel

A. Wisniewski · J. Beddoes

Received: 22 April 2008 / Accepted: 5 June 2008 / Published online: 24 June 2008

Abstract Creep at 700 °C/196 MPa and 900 or 925 °C/27.4 MPa of 21Cr–4Ni–9Mn austenitic stainless steel is determined as a function of the heat treatment. The heat treatment variation involves altering the solution heat treatment cooling rate from water quenching to cooling at 6 or 4 °C/min causing: serrated grain boundaries versus planar grain boundaries, coarser intergranular carbides, and discontinuous precipitation of grain boundary reaction zones. Water quenching causes improved creep resistance. Creep fracture and cracking is intergranular. Coarse intergranular carbides and grain boundary reaction zones cause premature void formation and cracking, this damage leading to an accelerating creep rate and lowering creep resistance of the more slowly cooled conditions. During creep, grain boundary serrations, which may otherwise contribute to improved creep, are eliminated. Determining the individual influence of grain boundary serrations on creep requires a detailed investigation of various heat treatment parameters to prevent concurrent formation of grain boundary reaction zones and serrations.

Introduction

21Cr–4Ni–9Mn (21-4N) austenitic stainless steel is widely used for exhaust valves in four stroke reciprocating engines, having been originally patented in 1950 [1]. This application requires good creep strength at the operating temperature of about 750 °C. 21-4N contains both high carbon (0.45–0.60 wt%) and high nitrogen (0.30–0.50 wt%), with the high Mn content improving the solubility of N, and both Mn and N stabilising the austenite structure [2]. The high carbon and nitrogen contents allow hardening via solution heat treatment in the range 1,160–1,200 °C and precipitation ageing usually at 750–850 °C [1, 2]. Like several other classes of elevated temperature structural alloys, including Ni base superalloys [3–5], Co base superalloys [6–8] and austenitic stainless steels [9], the grain boundary morphology of 21-4N can be altered from planar to serrated by modifying the heat treatment to include a controlled slow cooling rate from the solution heat treatment [10, 11]. The formation of serrations has been associated with: intergranular precipitation in Ni and Co base superalloys [5, 12–17]; a reduction in the misorientation angle between adjacent grains in a Ni base superalloy [18] and an austenitic stainless steel [19]; a reduction in the lattice distortional strain energy in stainless steels [20]; or the formation of grain boundary reaction zones with rod like carbides in Co base superalloys [8, 11, 21] and 21-4N [22–25].

Several mechanisms have been proposed to explain the formation of serrated grain boundaries in nickel base superalloys [13, 14, 18, 26] and stainless steels [9, 20], with controlled intergranular precipitation key to most mechanisms. The grain boundary precipitates in 21-4N are $M_{23}C_6$ carbides or Cr_2N nitrides [2]. In this steel, carbides or nitrides can precipitate as discrete particles along grain boundaries or as a grain boundary reaction (GBR) zone of lamellar nodules [27], due to discontinuous cellular precipitation [28]. The extent of GBR increases with increasing nitrogen and carbon content, with the nitrogen content having a greater influence on GBR formation [27]. The presence of 8–10% GBR is needed to sufficiently serrate the grain boundaries [22, 23], with this extent of GBR corresponding to the longest creep rupture life [29].

A. Wisniewski · J. Beddoes (✉)
Mechanical & Aerospace Engineering, Carleton University, 1125 Colonel By Drive, Ottawa, ON, Canada K1S 5B6
e-mail: jbeddoes@mae.carleton.ca

Serrated grain boundaries improve the creep resistance of several alloys, generally by increasing the creep rupture life and ductility [4, 7, 10, 11, 21, 30–33] by delaying the onset of tertiary creep. This result is most often attributed to serrations improving the creep damage tolerance by improving the cavitation resistance due to modified grain boundary carbide morphology [9, 34, 35], reducing the rate of grain boundary sliding or increasing resistance to grain boundary cracking [10, 11, 18, 24, 36]. Importantly, for 21-4N, serrations delay the onset of tertiary creep resulting in longer creep rupture life when creep is tested at 700 °C and 196 or 294 MPa, and 900 °C and 27.4 or 49 MPa, but serrations have no influence on the steady state creep rates at 700 °C [10].

An ongoing research program aims to determine the characteristics of grain boundary serrations and the influence on the creep behaviour of elevated temperature alloys, including 21-4N and modified Waspaloy, a wrought Ni base superalloy. Initial results for the latter alloy indicate that serrated grain boundaries most benefit creep resistance at high temperature and low stress [37]. Within this program, this paper presents the influence of controlled cooling from the solution heat treatment on the formation of grain boundary serrations in 21-4N and the subsequent effect on creep, including microstructural stability during extended creep loading.

Materials and experimental procedure

Material for this study was cut from 22 mm diameter hot rolled bars of 21-4N with a grain size of approximately 5 μm and the composition listed in Table 1 as determined by optical emission spectroscopy for the major elements.

Three heat treated conditions were prepared according to the thermal profiles of Table 2. The NGB—normal or planar, and SGB—serrated, heat treatment details follow those specified in Refs. [10, 11]. The SGB-M heat treatment is the same as the SGB heat treatment, but with a modified cooling rate from the solution heat treatment.

Tensile creep specimens were machined to a straight gauge length of 40.6 mm and diameter of 6.3 mm. Grooves were machined into specimen shoulders for attachment of a LVDT equipped high temperature extensometer with strain resolution of $\pm 1 \times 10^{-4}$. Creep testing was conducted in Satec M3 creep frames at a constant load and temperature, corresponding to an initial stress of 196 MPa at 700 °C or 27.4 MPa at 900 and 925 °C. The temperature, from thermocouples attached to the specimen shoulders, was controlled to ±1 °C. The creep load was applied all at once via a motorized drawhead, with strain measurement initiated prior to loading. During and immediately following loading strain, data was recorded every second, with this time interval gradually increasing to a maximum of 30 min as the test proceeded.

Metallographic samples for optical microscopy were prepared by polishing using diamond and alumina media and etched in a fresh mixture of equal parts of HNO_3, HCl, and H_2O at room temperature.

Table 2 Heat treatment details

Condition	Heat treatment
NGB	1 h/1,200 °C WQ + 30 h/700 °C AC + 30 h/1,000 °C AC
SGB	1 h/1,200 °C FC to 1,030 °C WQ + 30 h/750 °C AC + 3 h/1,000 °C AC
SGB-M	1 h/1,200 °C CC to 1,030 °C WQ + 30 h/750 °C AC + 3 h/1,000 °C AC

FC, furnace cool (6 °C/min); CC, control cool (4 °C/min); WQ, water quench; AC, air cool

Results

Heat treated microstructures

Figure 1 illustrates the microstructures of the three heat treated conditions after cooling from the solution heat treatment. All three conditions have an average grain size of between 90 and 110 μm. The grain boundary structure is most evident prior to ageing and does not significantly change during subsequent ageing. The NGB condition, Fig. 1a, has planar grain boundaries and is free of grain boundary reaction (GBR) zones. The grain boundary morphology of SGB, Fig. 1b, and the SGB-M, Fig. 1c are similar, both exhibiting well-defined serrations. Both the SGB and SGB-M contain GBR zones, the distributions of which are shown in Fig. 2. The image analysis of 30 areas on each sample shows that the SGB and SGB-M contain

Table 1 Nominal and actual composition of 21-4N (wt%)

	C	N	Cr	Mn	Ni	Mo	Si	P	S
Nominal [2]	0.45–0.60	0.30–0.50	20–23	7–10	3–5	–	0.25 max	–	–
Refs. [9, 10]	0.54	0.39	21.1	9.74	4.07	–	0.19	0.017	0.008
This study[a]	0.52	0.39	20.6	8.3	3.35	0.25	0.19	0.030	0.001

[a] Also contains 0.21Cu, 0.089V, 0.035Co, 0.029W, 0.020Nb

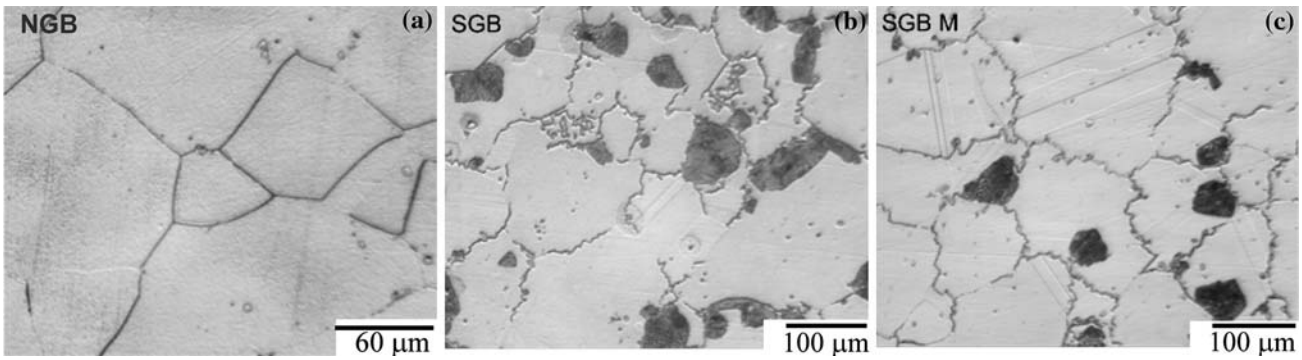

Fig. 1 Optical microstructures after solution heat treatment for (**a**) NGB, 1 h/1200 °C WQ; (**b**) SGB, 1 h/1,200 °C FC to 1,030 °C WQ and (**c**) SGB-M, 1 h/1,200 °C cool at 4 °C/min to 1,030 °C WQ

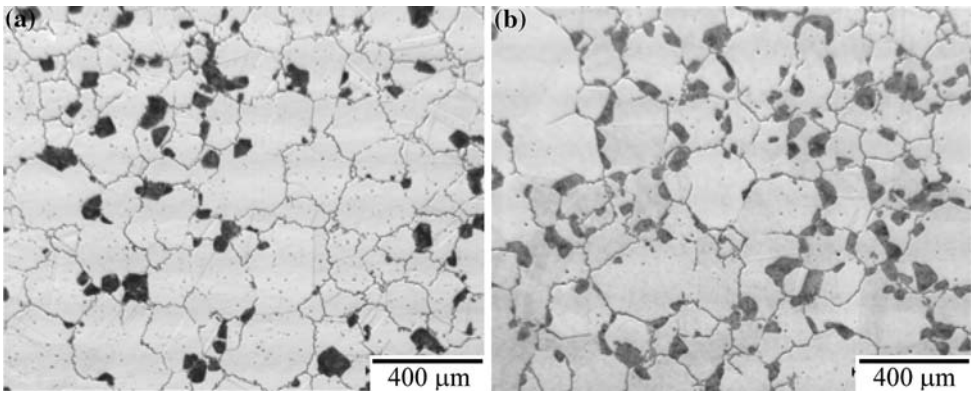

Fig. 2 Optical micrographs of the extent of GBR in the (**a**) SGB and (**b**) SGB-M conditions after solution heat treatment

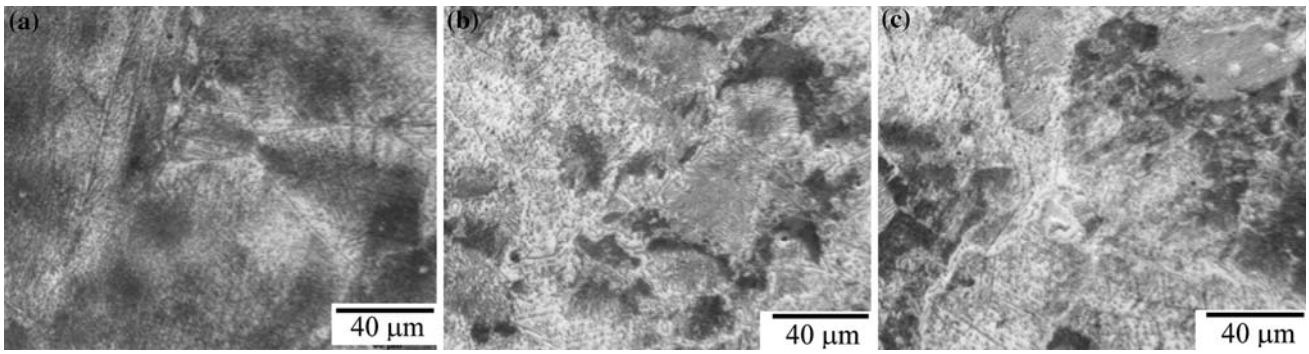

Fig. 3 Optical micrographs of the fully heat treated conditions: (**a**) NGB, (**b**) SGB and (**c**) SGB-M, showing microstructural homogeneity of each condition

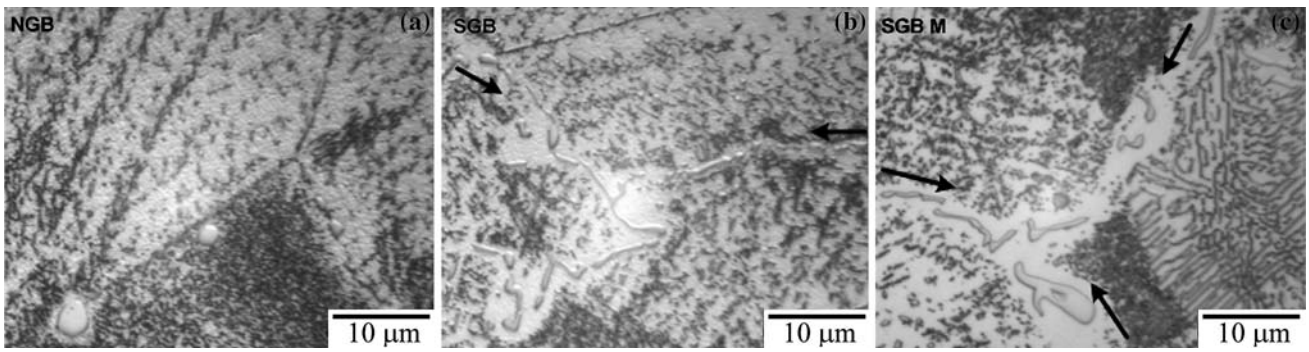

Fig. 4 Optical micrographs of the fully heat treated conditions: (**a**) NGB, (**b**) SGB and (**c**) SGB-M, showing grain boundary carbides in each condition. Arrows indicate grain boundary locations. Note the GBR zone evident in SGB-M on right side of micrograph

16% and 10% area fraction of GBR, respectively. These GBR zones are retained during ageing and as a result the SGB and SGB-M conditions exhibit more non-uniform microstructures compared to the NGB condition which contains no GBR, Fig. 3. A second important difference between the three microstructures is the presence of coarser grain boundary carbides in the SGB and SGB-M conditions, Fig. 4b and c, with only isolated coarse carbides in the NGB condition, Fig. 4a. Also evident in Fig. 4 is the presence of regions with a lower precipitate particle density adjacent to some grain boundary segments in the SGB and SGB-M conditions, likely due to greater local solute removal by the coarser carbides.

Creep properties

Figure 5 shows that at all temperature and stress test conditions the NGB condition with planar grain boundaries displays the best creep resistance. At 700 °C and 196 MPa, Fig. 5a, the NGB condition has a lower creep strain at all times to rupture, and a longer rupture life than SGB, but slightly shorter rupture life compared to SGB-M. These results differ from those presented in [10, 11] which show a clear benefit of a slower cool from the solution heat treatment causing grain boundary serrations in terms of both longer rupture life and a lower strain at all times to rupture.

Although at 900 °C and 27.4 MPa creep tests were interrupted prior to rupture, the results of Fig. 5b clearly indicate superior creep resistance of the NGB condition with planar grain boundaries. Again this result is contrary to that in [10, 11] which showed a longer rupture life for the condition with serrated grain boundaries. Moreover, it is evident that the creep life of the current results is much longer than that previously reported. For example, in Fig. 5b the NGB condition has a rupture life >2,000 h, while the corresponding 'N' condition of Fig. 6 in [10] or Fig. 5 of [11], with ostensibly the same composition, Table 1, and the same heat treatment, had a rupture life of only about 230 h. Importantly, the SGB-M condition with serrated grain boundaries has similar creep properties to the NGB condition with planar grain boundaries to the time extent tested, Fig. 5b.

Again at 925 °C and 27.4 MPa creep tests were interrupted prior to rupture, but nevertheless consistent with the other test temperatures and stresses, the results of Fig. 5c illustrate that the NGB condition exhibits superior creep resistance.

Creep fracture

For all microstructural and test conditions creep fracture is intergranular. Figure 6a shows a SEM secondary electron image of the NGB fracture surfaces clearly exhibiting

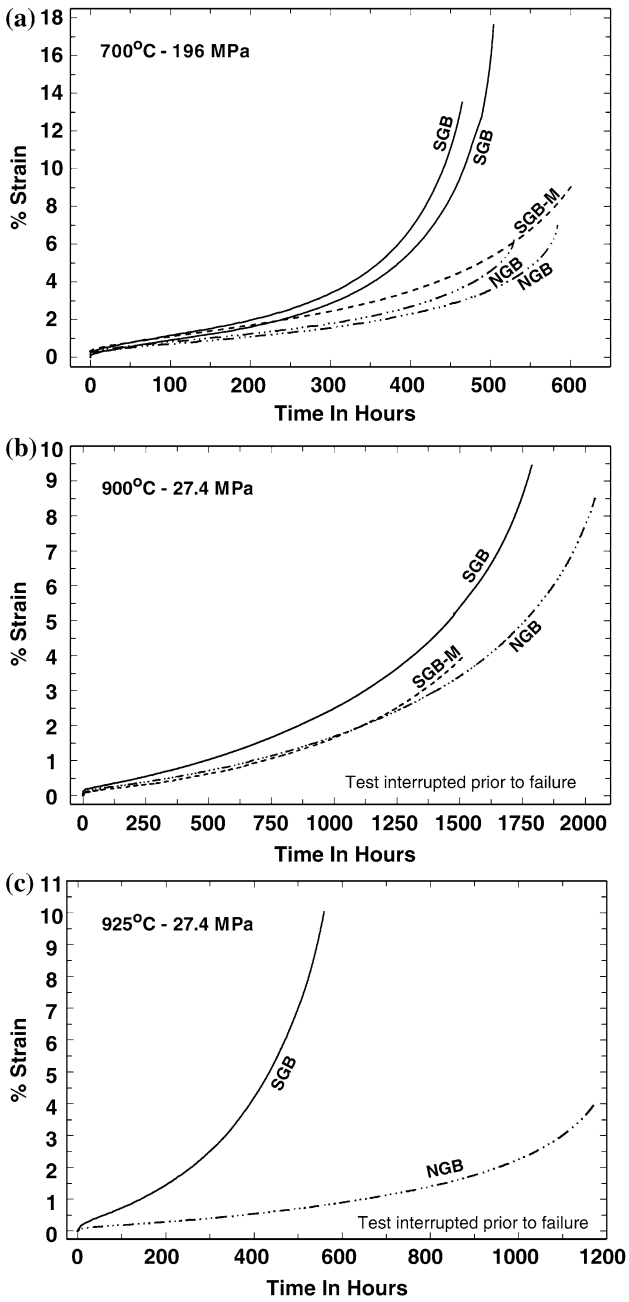

Fig. 5 Creep curves for three microstructural conditions tested at (**a**) 700 °C, 196 MPa; (b) 900 °C, 27.4 MPa and (**c**) 925 °C, 27.4 MPa

planar grain boundary facets. The fracture surfaces of samples with serrated grain boundaries have a dimpled appearance consistent with the serrated morphology, Fig. 6b. While creep tests at 900 and 925 °C were interrupted prior to rupture, intergranular cracking occurred during these tests, Fig. 7. As seen in Fig. 8, coarse carbides along grain boundaries can act as nuclei for void formation leading to intergranular cracking of the type shown in Fig. 7. Initiation of intergranular cracking is also associated with the GBR zones in the SGB condition, Fig. 9.

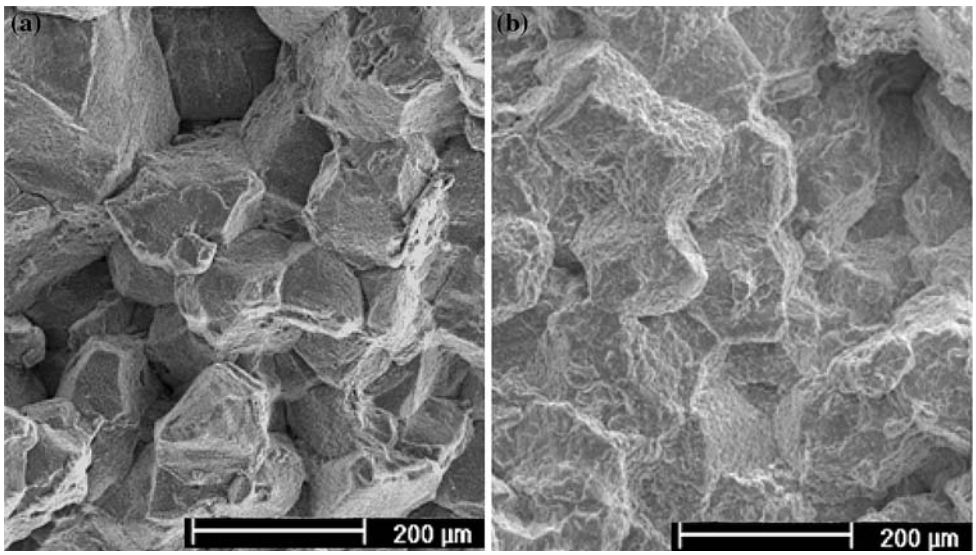

Fig. 6 SEM secondary images of the fracture surfaces after creep at 700 °C: 196 MPa, (**a**) NGB and (**b**) SGB-M

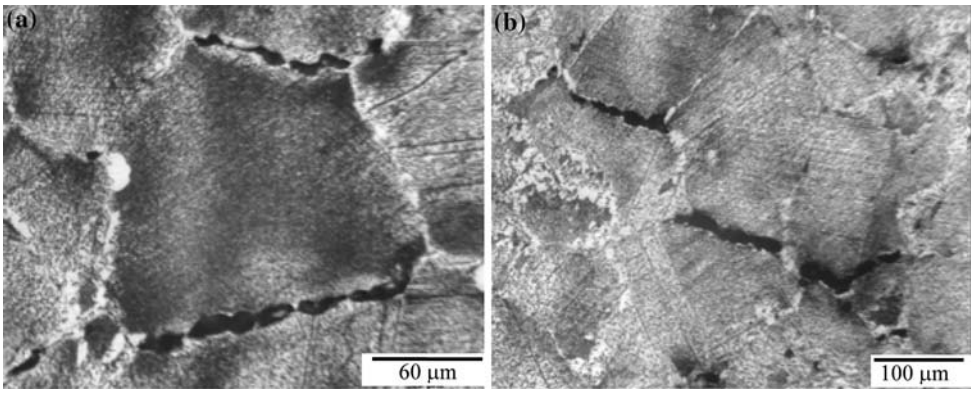

Fig. 7 Optical microscopy images of the intergranular cracking in the gauge length after creep of (**a**) NGB at 925 °C and 27.4 MPa, and (**b**) SGB-M at 900 °C and 27.4 MPa. Loading direction is vertical

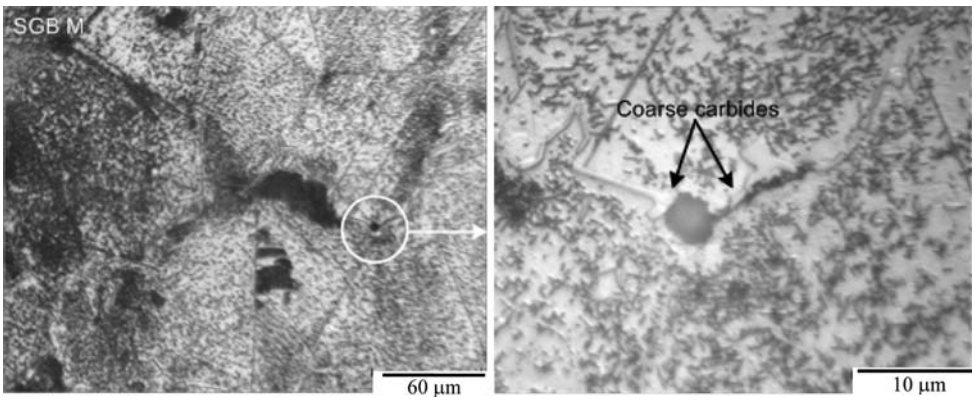

Fig. 8 Grain boundary cavities in the gauge length associated with coarse carbides after creep in SGB-M after creep at 700 °C and 196 MPa

Post-crept microstructures

After creep testing, microstructures in the gauge length of all three conditions were much more similar to each other than prior to creep. Intragranular precipitate structures after testing at 700 °C were virtually identical and both the SGB and SGB-M conditions contained portions of grain boundaries without serrations and nearly continuous carbides. Likewise, after testing at 900 °C, Fig. 10, the NGB and SGB conditions have very similar microstructures with uniform intragranular precipitation and coarse grain boundary carbides. After testing at 925 °C, grain boundary carbides in the NGB condition, Fig. 11a, are coarser than prior to creep testing, Fig. 4a, with discrete particles nearly continuous along grain boundaries. In the SGB condition, Fig. 11b, carbides are larger than in the NGB condition, Fig. 11a, and coarser than

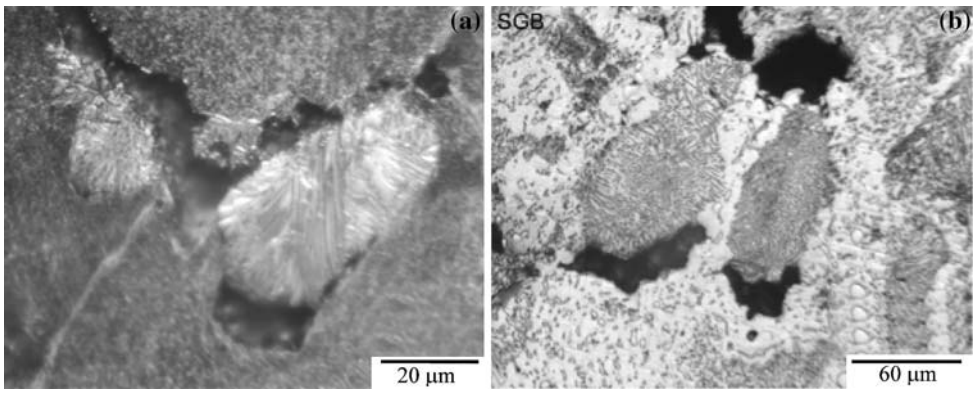

Fig. 9 Cracking in the gauge section associated with GBR in SGB after creep at (**a**) 700 °C and 196 MPa and (**b**) 900 °C and 27.4 MPa

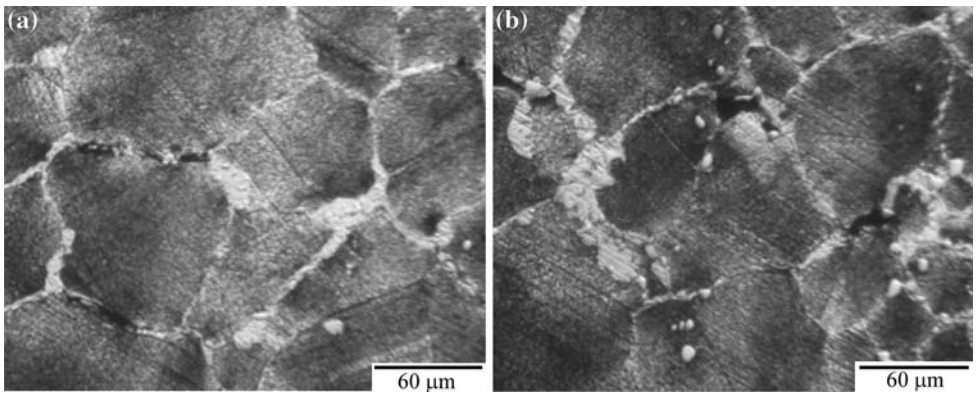

Fig. 10 Microstructures in the gauge section after creep at 900 °C and 27.4 MPa of (**a**) NGB and (**b**) SGB

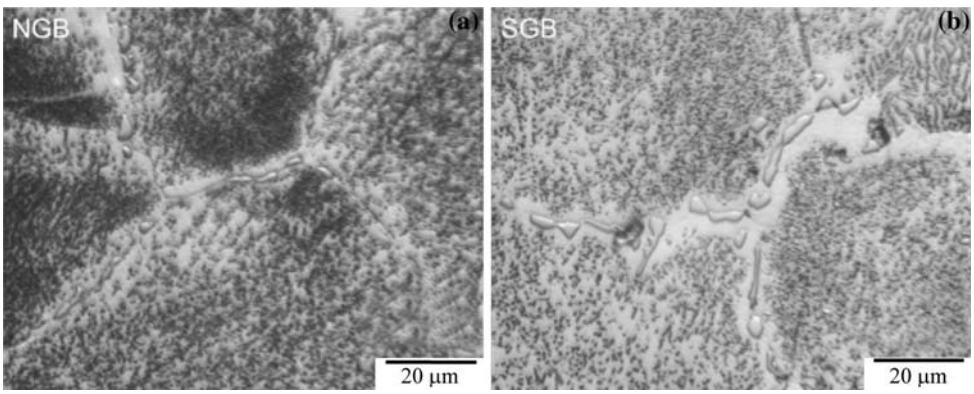

Fig. 11 Grain boundary carbide microstructures in the gauge section after creep at 925 °C and 27.4 MPa of (**a**) NGB and (**b**) SGB

prior to creep testing, with a distinct adjacent precipitate free zone. After creep testing at 900 and 925 °C, the serrated grain boundary configuration of the SGB and SGB-M conditions has been eliminated, Fig. 10b, and GBR zones are much less distinct.

Discussion

Heat treated microstructures

The SGB microstructure contains about 16% area fraction of GBR zones, Fig. 2a. This is in excess of the ideal amount for best creep resistance of 8–10% [29]. Although the heat treatment applied in this study (SGB) and [29] are ostensibly identical, likely the furnace cool from the solution heat treatment varies between this study and [29]. The furnace used in this study of 21-4N produced a power off furnace cooling rate of approximately 6 °C/min. By reducing the cooling rate from the solution heat treatment to 4 °C/min (SGB-M) the same 10% area fraction of GBR as [29] is achieved, Fig. 2(b).

The results indicate that a comparison of serrated and planar grain boundary microstructures of 21-4N is at best difficult, as the microstructures show significant other differences. This appears to be unavoidable since the GBR zones form concurrently with grain boundary serrations during controlled cooling from the solution heat treatment.

The NGB condition which is water quenched from the solution heat treatment is completely free of GBR, Fig. 1a, while the slowly cooled SGB and SGB-M conditions contain 16% and 10% GBR, respectively, Fig. 2, the presence of which leads to microstructural non-uniformity, Fig. 3. While the mechanism for the formation of grain boundary serrations has not been investigated in this study, it is likely that a precursor to the discontinuous cellular precipitation process responsible for the formation of GBR is at least partially responsible for the formation of serrations. The connection between GBR and serrations in 21-4N has been suggested elsewhere [22–25], making it incongruous to consider the impact on creep of GBR and serrations independently.

An additional important difference between the NGB condition with planar boundaries and the serrated grain boundary conditions of SGB and SGB-M is the degree of intergranular carbides, Fig. 4. Carbide coarsening occurs during the controlled slow cooling from the solution heat treatment.

Creep behaviour

In contrast to [10, 11] the results of Fig. 5 clearly show that the NGB microstructure with planar grain boundaries and no GBR exhibits the best creep properties. Consistent with [29] reducing the area fraction of GBR from 16% in SGB to 10% in SGB-M did result in an improvement to creep properties and even a slightly longer creep rupture life than the NGB condition when tested at 700 °C, but the NGB condition maintains an equivalent or lower creep strain at all times than either of the SGB or SGB-M conditions at all temperatures evaluated.

The results of Fig. 5b shows a much longer creep rupture life at 900 °C compared to those reported in [10, 11]. The reasons for this difference are not immediately clear. The dimensions of the creep test coupons in this study and [10, 11] are not significantly different and testing procedures appear to be similar. Comparison of the 21-4N used for [10, 11] and the current study, Table 1, indicates that with respect to the major substitutional additions of Cr, Ni and Mn and the interstitial additions of C and N the compositions are nearly identical. However, the 21-4N in the current study also contained minor additions of Mo, Cu, V, W and Co. The addition of Mo to austenitic stainless steels is known to improve creep properties [38] and increased levels of refractory elements such as V, W and Co would be expected to do likewise. It is not known whether specifically for 21-4N the levels of these minor element additions will result in the difference in creep properties at 900 °C.

Returning to the lack of improvement in creep properties from the serrated grain boundaries, there are several factors that may contribute to this result. A primary factor may be the instability of the microstructures with serrated grain boundaries. The microstructural instability is evident by comparing the 900 °C crept micrographs of Fig. 10, with those of the heat treated micrographs of Fig. 3. The crept NGB and SGB microstructures are virtually identical, with the SGB-M microstructure appearing very similar. The crept SGB microstructure exhibits a uniform distribution of intragranular precipitates, less well-defined GBR zones and planar grain boundaries, all features that differ from the heat treated microstructure.

A second factor contributing to the poor creep of the SGB and SGB-M conditions could be increased susceptibility to intergranular cracking. The controlled cooling from the solution heat treatment allows coarsening of the intergranular carbides as well as the formation of GBR zones. Figures 8 and 9 clearly indicate that void formation and intergranular cracking are associated with these microstructural features. Indeed, the SGB sample tested at 925 °C and 27.4 MPa contained secondary cracks almost exclusively at the GBR nodules. Therefore, the combination of coarser grain boundary carbides and GBR zones acting as crack initiation sites could explain the poor creep of the SGB and SGB-M conditions with respect to the NGB condition. It would also explain why creep at 900 °C and 27.4 MPa is dominated by the tertiary stage during which there is an accelerating creep strain rate. In essence, right from the start of creep testing the SGB and SGB-M conditions contain a larger number of potential crack initiation sites which cause an accelerating creep rate at an earlier time than the NGB condition, which only forms coarse grain boundary carbides as creep exposure accumulates, resulting in a delayed onset of tertiary creep. Consequently, in 21-4N the benefits of serrated grain boundaries, observed in other elevated temperature alloys, is outweighed in the SGB or SGB-M conditions by microstructural instability during creep exposure—including elimination of the serrations—and the lower resistance to void formation and intergranular cracking due to the presence of coarse carbides and GBR zones.

Summary and conclusions

For 21-4N, altering the heat treatment by changing the cooling rate from the solution heat treatment has a significant influence on the resulting microstructures and creep properties. Compared to water quenching, controlled cooling at 6 or 4 °C/min results in three microstructural differences: coarser intergranular carbides, serrated grain boundaries and grain boundary reaction zones consisting of lamellar carbides. The change from 6 to 4 °C/min alters the area fraction of grain boundary reaction zones from 16% to 10%.

The creep properties at 700 °C and 196 MPa, and 900 or 925 °C and 27.4 MPa depend on the cooling rate from the solution heat treatment, with water quenching resulting in the best creep resistance in terms of retarding the onset of tertiary creep. The reduced creep resistance resulting from controlled slow cooling from the solution heat treatment is due to the instability of grain boundary serrations during creep exposure, and intergranular cracking associated with grain boundary reaction zones and coarse carbides.

All three microstructural differences due to changing the cooling rate from the solution heat treatment from water quenching to slow controlled cooling have an impact on the subsequent creep properties. Therefore, to unequivocally draw conclusions about the influence of serrations on the creep of 21-4N will require a more detailed understanding of the influence of varying the solution heat treatment cooling rate on the formation of serrations, grain boundary reaction zones and carbide structure.

Acknowledgements This research was funded by the Natural Sciences and Engineering Research Council of Canada through the Discovery grant program. Thanks are due to Crucible Specialty Metals, Syracuse, New York,for supply of the 21-4N bars.

References

1. Beddoes GN (1992) Ironmak Steelmaking 19:290
2. Lula RA (1986) Manganese in stainless steels. The Manganese Centre, Paris
3. Koul AK, Immarigeon JP, Wallace W (1994) In: Koul AK, Parameswaran VR, Immarigeon JP, Wallace W (eds) Advances in high temperature structural materials and protective coatings. National Research Council Canada, Ottawa
4. Beddoes J, Wallace W (1980) Metallography 13:185. doi:10.1016/0026-0800(80)90015-4
5. Larson JM, Floreen S (1977) Metall Trans 8A:51
6. Tanaka M (1993) Z Metallk 84:51
7. Tanaka M, Iizuka H, Tagami M (1989) J Math Sci 24:2421. doi:10.1007/BF01174505
8. Tanaka M, Iizuka H, Ashihara F (1992) J Math Sci 27:2636. doi:10.1007/BF00540682
9. Hong HU, Nam SW (2003) J Math Sci 38:1535. doi:10.1023/A:1022989002179
10. Tanaka M, Miyagawa O, Sakaki T et al (1988) J Math Sci 23:621. doi:10.1007/BF01174696
11. Tanaka M, Iizuka H, Ashihara F (1987) Trans ISIJ 28:129
12. Koul AK, Thamburaj R (1995) Metall Trans 16A:17
13. Wu XJ, Koul AK (1997) Adv Perform Mater 4:409. doi:10.1023/A:1008648628507
14. Koul AK, Gessinger GH (1983) Acta Metall 31:1061. doi:10.1016/0001-6160(83)90202-X
15. Larson JM (1976) Metall Trans 7A:1497
16. Letellier L, Guttmann M, Blavette D (1994) Philos Magn Lett 70:189. doi:10.1080/09500839408240974
17. Henry MF, Yoo YS, Yoon DY et al (1993) Metall Trans 24A:1733
18. Danflou HL, Marty M, Walder A (1992) Proceedings of the 7th International Symposium Superalloys 63
19. Hyun UH, Nam SW (2001) Z Metallkunde 92:1331
20. Kim KJ, Ginsztler J, Nam SW (2005) Mater Lett 59:1439. doi:10.1016/j.matlet.2004.12.050
21. Iizuka H, Tanaka M (1986) J Math Sci 21:2803. doi:10.1007/BF00551493
22. Iizuka H, Tanaka M, Ashihara F (1991) J Eng Mat Tech 113:9. doi:10.1115/1.2903389
23. Iizuka H, Tanaka M, Miyagawa O et al (1096) Trans Jpn Inst Met 27:851
24. Iizuka H, Tanaka M (1989) Trans Jpn Soc Mech Eng Part A 55:1469
25. Iizuka H, Tanaka M, Ashihara F (1988) Trans Jpn Soc Mech Engineers Part A 54:1317
26. Larson JM, Floreen S (1977) Metall Trans 8A:51
27. Tanaka M, Miyagawa O, Fujishiro D (1977) J Jpn Inst Met 41:11
28. Knutsen RD, Lang CI, Basson JA (2004) Acta Math 52:2407. doi:10.1016/j.actamat.2004.01.031
29. Tanaka M, Miyagawa O, Sakaki T et al (1979) J ISIJ 65:939
30. Yoshiba M, Miyagawa O (1985) Trans ISIJ 26:69
31. Chang M, Koul AK, Au P et al (1994) J Mat Eng Perf 3:356. doi:10.1007/BF02645332
32. Tanaka M, Iizuka H, Tagami M (1989) J Math Sci 24:1623. doi:10.1007/BF01105682
33. Tanaka M, Iizuka H (1990) z Metallkunde 81:149
34. Kim KJ, Hong UH, Min KS et al (2004) Mater Sci Eng A 387–389:531. doi:10.1016/j.msea.2004.01.126
35. Kim KJ, Hong UH, Min KS et al (2004) Acta Metab Sin 17:632
36. Tanaka M, Iizuka H, Ashihara F (1988) J Math Sci 23:3827. doi:10.1007/BF01106799
37. Wisniewski A, Beddoes J (2008) Mater Sci Eng A (in press)
38. Sourmail T (2001) Mat Sci Tech 17:1